

## Scalings of Rayleigh-Taylor Instability at Large Viscosity Contrasts in Porous Media

N. Sabet<sup>1</sup>, H. Hassanzadeh<sup>1</sup>, A. De Wit<sup>2</sup>, and J. Abedi<sup>1</sup>

<sup>1</sup>*Department of Chemical and Petroleum Engineering, Schulich School of Engineering, University of Calgary, T2N 1N4 Calgary, Alberta, Canada*

<sup>2</sup>*Université libre de Bruxelles (ULB), Nonlinear Physical Chemistry Unit, Faculté des Sciences, CP231, 1050 Brussels, Belgium*

 (Received 9 June 2020; accepted 25 January 2021; published 5 March 2021)

The scalings of the Rayleigh-Taylor instability are studied numerically for porous media flows when the denser fluid lying on top of the less dense one is also much more viscous. We show that, above a critical value of the viscosity ratio  $M$ , a symmetry breaking of the buoyancy-driven fingers is observed as they extend much further downward than upward. The asymmetry ratio scales as  $M^{1/2}$  while the asymptotic flux across the initial contact line, quantifying the mixing between the two fluids, scales as  $M^{-1/2}$ . A new fingering mechanism induced by large viscosity contrasts is identified and shows good agreement with experimentally observed dynamics.

DOI: [10.1103/PhysRevLett.126.094501](https://doi.org/10.1103/PhysRevLett.126.094501)

Rayleigh-Taylor (RT) instability is a buoyancy-driven instability developing when a denser fluid is accelerated against a less dense fluid. It favors mixing between the two fluids and is genuinely observed in inertial confinement fusion [1–3], plasmas [4], liquid films [5], material deformation [6], oceanography [7], and astrophysics [8,9], to name a few. Motivated by the interest to control this mixing, universal scalings, quantifying the interpenetration of the two fluids as a function of the acceleration or the density and viscosity differences across the interface, are of tantamount importance.

Scalings of RT instability for porous media flows have also attracted much attention recently due to its ubiquity in applications as diverse as suspension of active particles [10], granular flows [11], CO<sub>2</sub> sequestration [12], geological flows [13,14], and enhanced oil recovery [15], among others. Experimental studies on miscible RT convection in porous media have shown that the mean amplitude and wavelength of fingers scale with  $t$  and  $t^{1/2}$ , respectively [16,17]. Theoretical works have further explored the effect on scalings of convective versus diffusive mixing modes [18], differential diffusion [19,20], chemical reactions [21] as well as the validity of 2D models in describing the flow dynamics [22], the characterization of diffusive, convective, and shutdown regimes [23], and the universality of the scalar dissipation rate [14,24].

In most works, the viscosity is supposed to be equal in both fluids while, in reality, the viscosities of fluid pairs with different densities are also typically different. Even though a viscosity contrast may delay the onset of the RT instability [25], the up-down symmetry of the growing fingers was shown numerically to be preserved within the limited range of viscosity ratios ( $M \leq 20$ ) investigated [15].

Despite the fact that an experimental study on the leaching of extremely viscous oils by a miscible solvent suggests that new dynamics are observed when large viscosity contrasts exist [26,27], the influence of viscosity on the RT instability remains largely unknown.

Through 2D numerical simulations, we show here for porous media flows that large viscosity contrasts profoundly affect the RT instability as a breaking of symmetry of the buoyancy-driven fingers occurs above a critical value of the viscosity ratio  $M$ . The fingers extend then preferably in the fluid of lower viscosity, which has an impact on the mixing. We characterize the effect of viscosity contrast on the RT convection across a wide range of viscosity ratios (up to  $M \approx 3000$ ) and obtain new scaling relations, characterizing the fingers spreading around the initial interface of fluids. In particular, we derive scalings of the spreading rates of fluids and of their convective mass flux as a function of  $M$ . We also introduce a new fingering mechanism observed at large viscosity ratios, which enlightens the hitherto unexplained previous experiments [26].

We consider a 2D, homogeneous, and isotropic porous medium of dimensional width  $W^*$  and height  $H^*$ . A denser and more viscous fluid containing a solute in dimensional concentration  $c_2^*$  and of density  $\rho_2^*$  and viscosity  $\mu_2^*$  overlies another miscible, less dense, and less viscous fluid with density  $\rho_1^*$  ( $< \rho_2^*$ ) and viscosity  $\mu_1^*$  ( $< \mu_2^*$ ) where, without loss of generality,  $c_1^* = 0$ . This stratification leads to an RT instability as the density decreases along the direction of gravity. For bulk fluids with turbulent mixing, 3D effects might be important [28]. However, for RT convection in porous media or Hele-Shaw cells where the magnitude of flow velocities are small, similar key physics have been observed in 2D and 3D simulations [15,22].

We define the scales  $c_2^*$ ,  $v_{ch}^*$  ( $= K^* \Delta \rho^* g / \mu_1^*$ ),  $\phi D^* / v_{ch}^*$ ,  $\phi^2 D^* / v_{ch}^{*2}$ ,  $\mu_1^*$ ,  $\Delta \rho^* (= \rho_2^* - \rho_1^*)$ , and  $\mu_1^* \phi D^* / K^*$  for concentration, velocity, space, time, viscosity, density, and pressure, respectively, where  $K^*$  is the permeability,  $g$  the gravitational acceleration,  $\phi$  the porosity, and  $D^*$  the effective diffusion coefficient. Using these scales, the dimensionless form of the governing equations, under the Boussinesq approximation, is

$$\nabla \cdot \mathbf{v} = 0, \quad (1)$$

$$\mu(c) \mathbf{v} = -\nabla p - \rho(c) \hat{\mathbf{k}}, \quad (2)$$

$$c_t = -\mathbf{v} \cdot \nabla c + \nabla^2 c, \quad (3)$$

where  $c$  is the concentration of the solute ruling density and viscosity,  $\mathbf{v} = (u, w)$  is the Darcy velocity vector,  $p$  is the pressure, and  $\hat{\mathbf{k}}$  is the unit vector in the  $z$  direction (positive upward).

The dimensionless height and width of the numerical domain become  $Ra$  and  $Ra/A$ , respectively, where  $Ra = v_{ch}^* H^* / \phi D^*$  is the Rayleigh number and  $A = H^* / W^*$  is the aspect ratio of the domain. The initial position of the miscible interface is at  $z = 0$  such that  $-Ra_d \leq z \leq Ra_u$  where  $Ra_d = 3Ra/4$  and  $Ra_u = Ra/4$  are the initial dimensionless heights of the bottom and top fluids, respectively [29]. The horizontal axis is defined as  $0 \leq x \leq Ra/A$ . Following previous works [15,25,33], we adopt linear and exponential relations for the concentration dependence of the density and viscosity as  $\rho(c) = c$  and  $\mu(c) = \exp(Rc)$ , respectively, where  $R = \ln(M)$  is the log-viscosity ratio with  $M = \mu_2^* / \mu_1^*$  being the ratio of viscosities.

The governing equations can be expressed in terms of the stream function  $[(u, w) = (-\psi_z, \psi_x)]$  as

$$\nabla^2 \psi = -\nabla c \cdot [R \nabla \psi + e^{-Rc} \hat{\mathbf{i}}], \quad (4)$$

$$c_t = [\nabla \psi \times \nabla c] \cdot \hat{\mathbf{j}} + \nabla^2 c, \quad (5)$$

where  $\hat{\mathbf{i}}$  and  $\hat{\mathbf{j}}$  are the unit normal vectors in the  $x$  direction and in the direction perpendicular to the  $xz$  plane, respectively. The initial conditions are  $[c, \psi](x, z, t = 0) = [\mathbf{H}(z), 0]$  where  $\mathbf{H}$  is the Heaviside step function. No-flow and periodic boundary conditions are applied in the  $z$  and  $x$  directions, respectively.

To integrate the governing equations, we employ a hybridization of pseudospectral and compact finite difference methods. In this regard, the  $z$  and  $x$  derivatives are estimated using 4th and 6th-order compact finite difference [30] and fast Hartley transform [31], respectively. Time stepping is performed using the third-order semi-implicit Adam-Bashforth Adam-Moulton method. To achieve numerical stability at each time step for large viscosity contrasts, an under-relaxation scheme is employed [29].

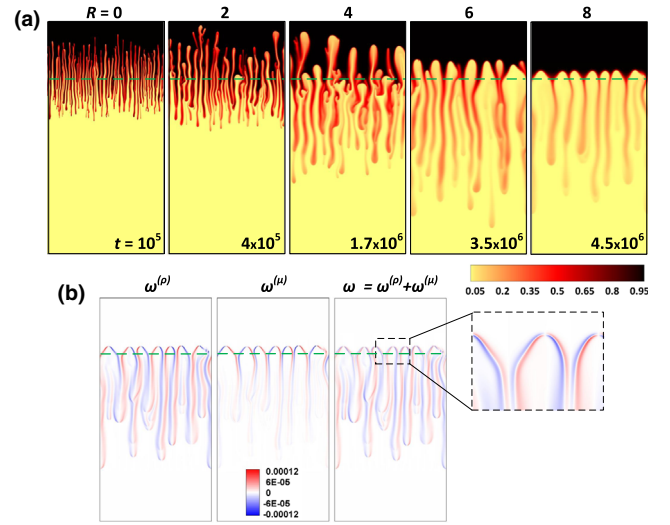


FIG. 1. (a) Concentration field at the time shown on the panel for  $Ra = 2 \times 10^5$  at different log-viscosity ratios  $R$ . As  $R$  increases, the up-down symmetry of fingering breaks. The dashed green line shows the initial location of the interface. (b) Density component of the vorticity field  $\omega^{(\rho)}$ , its viscosity component  $\omega^{(\mu)}$ , and the overall vorticity field  $\omega$  for  $R = 8$ .

The code was parallelized using OpenMP. For  $10^4 \leq Ra \leq 2 \times 10^5$ , the number of grid points are between  $\sim 25 \times 10^4$  and  $\sim 2 \times 10^7$ . The time step satisfies both the CFL condition (with a coefficient of 0.4) and the numerical accuracy limitations imposed by diffusive terms. The code was tested against the results of Ref. [15] with good agreement.

Figure 1(a) shows snapshots of the concentration field for  $Ra = 2 \times 10^5$  and different values of  $M$ , up to  $\sim 3000$ , corresponding to a log-viscosity ratio  $R = 8$ . As previously reported [15], for small values of  $R$  ( $\leq 3$ ) and in the absence of vertical throughflow, upward and downward fingers grow at the same rate, and an up-down symmetry of the growing fingers is observed. This symmetry, however, breaks at greater viscosity ratios, the downward fingers becoming more prominent as  $R$  increases. At extremely large viscosity ratios ( $R = 8$ ), the fingering becomes almost one-sided as the upward fingers grow at a much smaller rate than the downward fingers. Figure 1(a) also reveals that, as the viscosity increases, the rate of fluid mixing is suppressed and the wavelength of the growing fingers increases. This weakening effect was also observed for the onset of convection in porous media [25,33].

To understand why convection is mitigated and why the fingering asymptotes toward one side as  $R$  increases, we analyze the vorticity field, written in 2D as  $\omega = c_x / \mu + R(wc_x - uc_z)$ . The vorticity field can be decomposed into density and viscosity counterparts as  $\omega^{(\rho)} = c_x / \mu [= \rho_x / \mu]$  and  $\omega^{(\mu)} = R(wc_x - uc_z) [= (w\mu_x - u\mu_z) / \mu]$ , respectively. The density component of vorticity  $\omega^{(\rho)}$ , which is the main driving force behind the

growth of the fingers, is inversely proportional to the local value of viscosity. In other words, as the viscosity of the mixing layer increases, the driving force for buoyancy-driven convection is weakened, and therefore, the growth of convective fingers is delayed (stabilization effect of viscosity) [33].

To gain insight into the observed asymmetry at high values of  $R$ , we plot the density and viscosity contributions of the vorticity field, along with its overall value for  $Ra = 2 \times 10^5$  and  $R = 8$  in Fig. 1(b). It is seen that the vorticity field for downward plumes is determined mainly by the transverse density gradients in  $\omega^{(\rho)}$ . However, since  $\omega^{(\rho)}$  is inversely proportional to viscosity, its strength is weakened as  $R$  increases. For upward plumes, the density and viscosity components of the vorticity act in opposite directions [compare the blue and red colors in the contours of Fig. 1(b)]. At small values of  $R$  (not shown here),  $\omega^{(\rho)}$  is dominant and  $\omega^{(\mu)}$  acts weakly in the opposite direction toward its stabilization. However, as  $R$  increases, the strength of  $\omega^{(\mu)}$  becomes more comparable to  $\omega^{(\rho)}$ , and as seen in Fig. 1(b), the overall vorticity field is significantly suppressed around the rising plumes.

The upward and downward spreading lengths can be, respectively, defined as  $L_u = 3 \int_0^{Ra_u} z(1 - \bar{c})dz / \int_0^{Ra_u} (1 - \bar{c})dz$  and  $L_d = 3 \int_{-Ra_d}^0 z\bar{c}dz / \int_{-Ra_d}^0 \bar{c}dz$ , where  $\bar{c}$  is the transverse average of the concentration [15].  $L_u$  ( $L_d$ ) quantifies the penetration length of the bottom (top) fluid into the top (bottom) one. The temporal evolution of  $L/Ra$  for  $Ra = 10^5$  and  $R = 6$  is given in Fig. 2(a). Initially, the interface is uniform, and diffusion is the dominant transport mechanism such that  $L_{u,dif} = L_{d,dif} = 3\sqrt{\pi}t/2$ . Once buoyancy-driven convection sets in, both upward and downward spreading lengths begin to increase and asymptote toward a growth regime proportional to  $t$  with slopes  $U_u$  and  $U_d$ , respectively [15].

Figure 2(b) shows the asymptotic spreading rates,  $U_u$  and  $U_d$  versus  $M$  for various values of  $Ra$ . At large

Rayleigh numbers where the boundaries have no impact on the mixing, the spreading rates are independent of  $Ra$  [14,34]. Figure 2(b) also shows that, at small viscosity ratios,  $U_u \approx U_d \sim M^{-2/3}$ , as there is an up-down symmetry of fingering [15]. At larger values of  $M$ , however, the fingering becomes asymmetric with  $U_u$  still scaling as  $M^{-2/3}$ , while  $U_d$  switches from an  $M^{-2/3}$  trend at low  $M$  values to an  $M^{-1/6}$  scaling above a critical value of  $M$  ( $M_c$ ). This bifurcation in scaling is clearly seen in Fig. 2(c) giving the asymmetry ratio  $\eta = U_d/U_u$  versus  $M$ . At smaller values of  $M$ ,  $\eta \approx 1$ , but above a critical value ( $M_c \approx 20$ ), it increases monotonically as  $M^{1/2}$  ( $= M^{-1/6}/M^{-2/3}$ ).

Scalings of the convective mass flux, characterizing the long-term mixing of fluids [14], have been investigated for Rayleigh-Bénard convection [35,36], partially miscible systems [12,37], and fluid pairs with nonmonotonic density profile [38–40]. For partially miscible systems with a solute diffusing into the domain through one of the boundaries (e.g.,  $\text{CO}_2$ -water systems), the mass flux can be obtained easily using the cumulative mass of the diffusing species in the host phase [14,35,37]. However, for miscible systems like the one described in this work, it is challenging to calculate the convective mass flux because the system is closed (i.e., there is no mass being added over time) [14]. Here, we compute the convective mass flux based on the time evolution of the average concentration within either the upper or the lower domain on the sides of the initial contact line.

Taking the average of Eq. (3) in the upper domain, we can write  $\langle c \rangle_t^+ = \langle -\mathbf{v} \cdot \nabla c + \nabla^2 c \rangle^+$  where  $\langle \dots \rangle^+ = A/(Ra Ra_u) \int_0^{Ra_u} \int_0^{Ra/A} \dots dx dz$ . Applying the boundary conditions gives us  $F = -Ra_u \langle c \rangle_t^+$  where  $F = (A/Ra) \int_0^{Ra/A} (wc - c_z)_{z=0} dx$  is the average dimensionless convective flux at the initial position of the interface between the two fluids ( $z = 0$ ) [29]. Similarly, we can define  $\langle \dots \rangle^- = A/(Ra Ra_d) \int_{-Ra_d}^0 \int_0^{Ra/A} \dots dx dz$  for

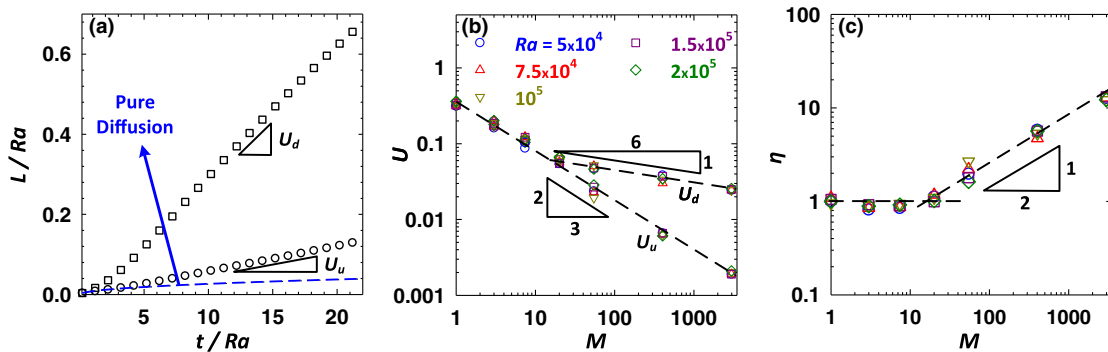


FIG. 2. (a) Normalized spreading length  $L/Ra$  versus  $t/Ra$  for  $Ra = 10^5$  and  $R = 6$ . The blue dashed curve shows the spreading rate for the pure diffusive case. After an initial diffusive regime, the spreading lengths asymptote toward a linear growth in time, with the upward  $U_u$  and downward  $U_d$  spreading rates, respectively. (b) Asymptotic upward and downward spreading rates as a function of the viscosity ratio  $M$  for various values of  $Ra$ . As  $M$  increases, the difference between  $U_u$  and  $U_d$  becomes more pronounced. (c) Asymmetry ratio  $\eta = U_d/U_u$  versus the viscosity ratio  $M$ .

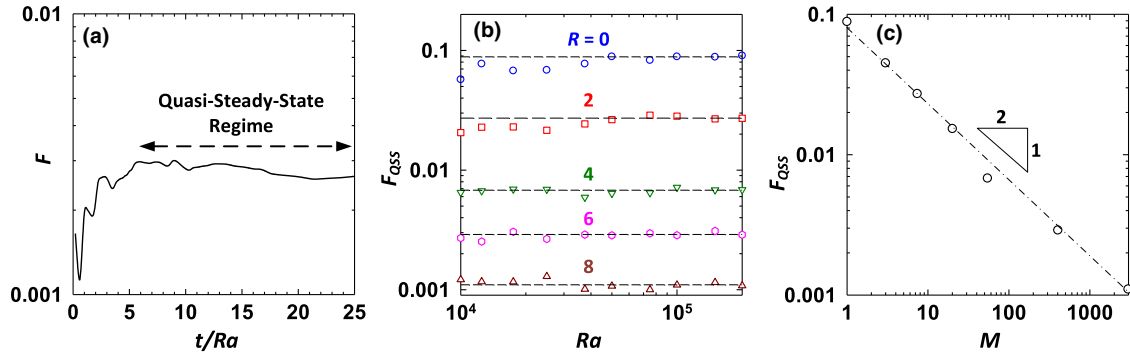


FIG. 3. (a) Convective mass flux as a function of rescaled time for  $Ra = 10^5$  and  $R = 6$ . After an initial diffusive regime, the flux reaches a quasi-steady-state regime. (b) Quasi-steady-state flux,  $F_{QSS}$ , versus  $Ra$  for various values of  $R$ . As  $Ra$  increases,  $F_{QSS}$  asymptotes toward a constant value,  $(F_{QSS}^\infty)$ . (c) Asymptotic flux  $F_{QSS}^\infty$  versus viscosity ratio  $M$  for large  $Ra$ .

the lower domain to get  $F = Ra_d \langle c \rangle_t^-$ . Using either of these expressions for flux leads to the same result due to the conservation of mass.

Figure 3(a) features the temporal evolution of the dimensionless convective flux  $F$  for  $Ra = 10^5$  and  $R = 6$ . After a transient diffusive decrease,  $F$  increases due to the enhanced mixing caused by convection and, eventually, reaches a quasi-steady-state regime in which the mass flux is nearly constant around the value  $F_{QSS}$  [14]. Figure 3(b) shows  $F_{QSS}$  as a function of  $Ra$  for various values of  $M$ . When  $Ra$  is large enough so that the top and bottom boundaries have no effect on the mixing,  $F_{QSS}$  becomes independent of  $Ra$  in agreement with classical scaling of convection [41]. Figure 3(c) shows that the asymptotic value of the flux  $F_{QSS}^\infty$  scales approximately as  $M^{-1/2}$  over the whole range of viscosity ratios scanned here. For viscosity ratios  $M$  beyond the limit investigated in this study, we speculate that similar dynamics to the case of  $R = 8$  would be observed, but over longer periods of time and with greater wavelengths. In this regard, the previous experimental observations of a fluid system with  $M \approx 10^7$  support this hypothesis [27]. Moreover, with insight from the analysis of critical Rayleigh number  $Ra_c$  for Rayleigh-Bénard convection [33], we anticipate that there is a certain value of  $M$ , beyond which,  $Ra_c$  surpasses  $Ra$ , and thus, the interfacial mixing is governed by diffusion.

A new dynamic observed during the RT convection of fluid pairs with large viscosity contrasts is the appearance of secondary fingers. Figure 4(a) shows a snapshot of the concentration field for  $Ra = 2 \times 10^5$  and  $R = 8$ . The enlarged frame shows that new small downward fingers begin to grow within the upward plumes because the upward spreading rate of fingers becomes so small at large viscosity ratios that the characteristic time of convection becomes comparable to that of diffusion. Since the upward velocities are minimal, a diffusive layer is formed below the edges of the fingers, which becomes unstable over time due to adverse density stratification. As a result, secondary downward fingers grow and then slide down on the edge of

the upward plumes. This observation is in agreement with experimental results of the RT convection between toluene and a viscous oil with a large viscosity ratio, as shown in Fig. 4(b) [26].

To summarize, we have shown that a viscosity contrast between two miscible fluids can drastically influence their mixing properties when an RT instability destabilizes their stratification. Strikingly, the buoyancy-driven fingers experience a symmetry breaking when the viscosity ratio  $M$  becomes larger than a critical value  $M_c$  of about 20 ( $R_c \approx 3$ ). The asymptotic growth rate of the upward growing plumes  $U_u$  scales as  $M^{-2/3}$  throughout the 3 orders of magnitude of  $M$  scanned while the downward mixing rate  $U_d$  slows down from a  $M^{-2/3}$  to a  $M^{-1/6}$  scaling across  $M_c$ . The asymmetry ratio  $\eta = U_d/U_u$  is more or less equal to 1 below  $M_c$  and bifurcates toward an  $M^{1/2}$  scaling above it. The asymmetry of the upward and downward fingers observed in this work is analogous to spike-bubble asymmetry in turbulent RT mixing of fluids at

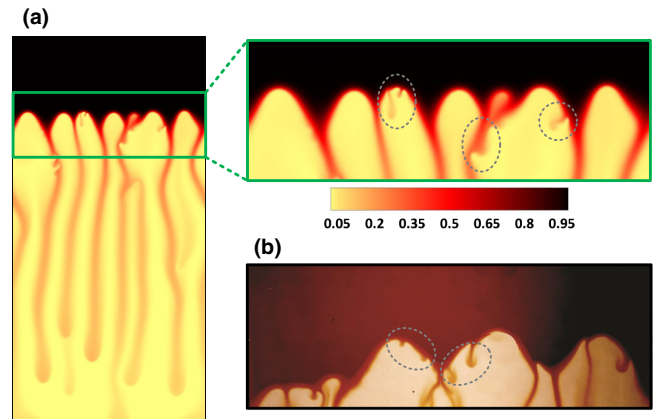


FIG. 4. (a) Concentration field for  $Ra = 2 \times 10^5$  and  $R = 8$ . Secondary fingers are observed within the upward plumes. (b) Snapshot of a Hele-Shaw experiment for the RT convection of an extremely viscous oil above toluene with  $R \approx 10.7$  [26] (used with permission).

large density ratios [42]. Our results reveal that the presence of a large density difference is not necessary for symmetry breaking of buoyancy-driven fingers in RT convection and this asymmetry can also be caused by large viscosity contrast of the fluids, even at the limit of Boussinesq approximation. The asymptotic convective flux scales like  $M^{-1/2}$  showing that an increase in the viscosity contrast acts against the quality of mixing. Moreover, a new mechanism, caused by a local instability of the diffusive boundary layer, triggers secondary fingers within the tips of upward plumes that are blocked by the viscosity contrast, in agreement with experiments. Our results pave the way for more realistic scalings of mixing between two fluids of different density and viscosity, as is genuinely the case in many applications. They also suggest that the quality of mixing between two fluids can be controlled via a careful choice of their relative viscosities.

We acknowledge financial support of NSERC, Mitacs, Killam Trusts, Alberta Innovates, and all member companies of SHARP Research Consortium. A. D. thanks FRS-FNRS for financial support of the PDR-CONTROL project.

- 
- [1] H. Zhang, R. Betti, R. Yan, D. Zhao, D. Shvarts, and H. Aluie, *Phys. Rev. Lett.* **121**, 185002 (2018).
- [2] J. P. Sauppe, S. Palaniyappan, B. J. Tobias, J. L. Kline, K. A. Flippo, O. L. Landen, D. Shvarts, S. H. Batha, P. A. Bradley, E. N. Loomis *et al.*, *Phys. Rev. Lett.* **124**, 185003 (2020).
- [3] Y. Zhou, *Phys. Rep.* **720–722**, 1 (2017).
- [4] B. Khiar, G. Revet, A. Ciardi, K. Burdonov, E. Filippov, J. Béard, M. Cerchez, S. Chen, T. Gangolf, S. Makarov *et al.*, *Phys. Rev. Lett.* **123**, 205001 (2019).
- [5] H. N. Yoshikawa, C. Mathis, S. Satoh, and Y. Tasaka, *Phys. Rev. Lett.* **122**, 014502 (2019).
- [6] A. Krygier, P. Powell, J. McNaney, C. Huntington, S. Prisbrey, B. Remington, R. Rudd, D. Swift, C. Wehrenberg, A. Arsenlis *et al.*, *Phys. Rev. Lett.* **123**, 205701 (2019).
- [7] R. W. Schmitt, *Annu. Rev. Fluid Mech.* **26**, 255 (1994).
- [8] A. Traxler, P. Garaud, and S. Stellmach, *Astrophys. J. Lett.* **728**, L29 (2011).
- [9] Y. Zhou, *Phys. Rep.* **723–725**, 1 (2017).
- [10] C. J. Miles, A. A. Evans, M. J. Shelley, and S. E. Spagnolie, *Phys. Rev. Lett.* **122**, 098002 (2019).
- [11] U. D’Ortona and N. Thomas, *Phys. Rev. Lett.* **124**, 178001 (2020).
- [12] H. Hassanzadeh, M. Pooladi-Darvish, and D. W. Keith, *AIChE J.* **53**, 1121 (2007).
- [13] G. F. Davies and M. A. Richards, *J. Geol.* **100**, 151 (1992).
- [14] J. J. Hidalgo, J. Fe, L. Cueto-Felgueroso, and R. Juanes, *Phys. Rev. Lett.* **109**, 264503 (2012).
- [15] O. Manickam and G. M. Homsy, *J. Fluid Mech.* **288**, 75 (1995).
- [16] R. A. Wooding, *J. Fluid Mech.* **39**, 477 (1969).
- [17] J. Fernandez, P. Kurowski, P. Petitjeans, and E. Meiburg, *J. Fluid Mech.* **451**, 239 (2002).
- [18] S. S. Gopalakrishnan, J. Carballido-Landeira, A. De Wit, and B. Knaepen, *Phys. Rev. Fluids* **2**, 012501(R) (2017).
- [19] S. S. Gopalakrishnan, J. Carballido-Landeira, B. Knaepen, and A. De Wit, *Phys. Rev. E* **98**, 011101(R) (2018).
- [20] S. M. Jafari Raad, H. Hassanzadeh, and J. Ennis-King, *Water Resour. Res.* **55**, 4030 (2019).
- [21] A. De Wit, *Annu. Rev. Fluid Mech.* **52**, 531 (2020).
- [22] J. Martin, N. Rakotomalala, and D. Salin, *Phys. Fluids* **14**, 902 (2002).
- [23] M. De Paoli, F. Zonta, and A. Soldati, *Phys. Rev. Fluids* **4**, 023502 (2019).
- [24] M. De Paoli, V. Giurgiu, F. Zonta, and A. Soldati, *Phys. Rev. Fluids* **4**, 101501(R) (2019).
- [25] S. Pramanik, T. K. Hota, and M. Mishra, *J. Fluid Mech.* **780**, 388 (2015).
- [26] I. J. Mokrys, The rise of interfering solvent chambers, Master’s thesis, University of Calgary, 1989.
- [27] R. Butler, I. Mokrys, and P. Herrera, *AOSTRA J. Res.* **2**, 147 (1985).
- [28] Y. Zhou, T. T. Clark, D. S. Clark, S. G. Glendinning, M. A. Skinner, C. M. Huntington, O. A. Hurricane, A. M. Dimits, and B. A. Remington, *Phys. Plasmas* **26**, 080901 (2019).
- [29] See Supplemental Material at <http://link.aps.org/supplemental/10.1103/PhysRevLett.126.094501>, which includes Refs. [30–32], for more details on the schematic of the problem, numerical methodology, and convective flux derivations.
- [30] S. K. Lele, *J. Comput. Phys.* **103**, 16 (1992).
- [31] R. N. Bracewell, *Proc. IEEE* **72**, 1010 (1984).
- [32] M. Islam and J. Azaiez, *Int. J. Numer. Methods Fluids* **47**, 161 (2005).
- [33] N. Sabet, H. Hassanzadeh, and J. Abedi, *AIChE J.* **64**, 1083 (2018).
- [34] V. Loodts, L. Rongy, and A. De Wit, *Chaos* **24**, 043120 (2014).
- [35] D. R. Hewitt, J. A. Neufeld, and J. R. Lister, *Phys. Rev. Lett.* **108**, 224503 (2012).
- [36] J. Otero, L. A. Dontcheva, H. Johnston, R. A. Worthing, A. Kurganov, G. Petrova, and C. R. Doering, *J. Fluid Mech.* **500**, 263 (2004).
- [37] M. A. Amooie, M. R. Soltanian, and J. Moortgat, *Phys. Rev. E* **98**, 033118 (2018).
- [38] S. Backhaus, K. Turitsyn, and R. E. Ecke, *Phys. Rev. Lett.* **106**, 104501 (2011).
- [39] J. A. Neufeld, M. A. Hesse, A. Riaz, M. A. Hallworth, H. A. Tchelepi, and H. E. Huppert, *Geophys. Res. Lett.* **37** (2010).
- [40] S. M. J. Raad and H. Hassanzadeh, *Phys. Rev. E* **92**, 053023 (2015).
- [41] L. N. Howard, in *Applied Mechanics* (Springer, New York, 1966), pp. 1109–1115.
- [42] Y. Zhou and W. H. Cabot, *Phys. Fluids* **31**, 084106 (2019).